

The effect of banded microstructures on the hole expansion behavior of hot-rolled steel

Xiaoyu Yang¹, Zhenli Mi^{1*}

¹Institute of Engineering Technology, University of Science and Technology Beijing, Beijing 100083, China

Abstract. Multiphase steels are widely used in automotive components due to their high strength and good local formability. The subtle hardness difference between microstructures makes multiphase steels exhibit excellent hole expansion performance. Our previous work insights that the distribution of microstructures changes the position of the serious plastic damage area on the punching hole edge which positively and decisively influences the hole expansion behavior of 800 MPa grade hot-rolled steels. In this work, two types of banded structures steels were constructed and their hole expansion behavior with and without pre-damage was investigated. The steels with banded ferrite and pearlite have excellent hole expansion performance due to their strong deformation capacity after necking. The cracks extending circumferentially along the direction of the banded structures and the higher toughness of the matrix are responsible for the higher hole expansion performance. The combination of ferrite and pearlite banded structures is an outstanding microstructure that has the potential to inspire the development of advanced high strength and hole expansion requirement multiphase steels.

Keywords: Multiphase steel; Hole expansion ratio; Banded structure; Pearlite.

1 Introduction

In recent years, the study of the local formability behavior of steels has gained particular importance [1, 2], as the fracture of metal structural components with local features, such as holes, cannot be adequately assessed using global formability evaluations such as forming limit curve predictions [3]. Additionally, these metal components typically fail without visual thinning or necking, which poses substantial risks to industrial production and application [4]. Hole expansion performance is a crucial indicator for evaluating the formability of components with holes [5]. The international standard ISO 16630 is widely used to assess the hole expansion performance [6, 7]. This evaluation method involves selecting an appropriate punching clearance based on the sheet thickness, and then punching a hole in a 90 × 90 mm specimen, followed by expanding it using a 60° conical punch. The test is terminated when a crack propagates through the entire thickness of the hole edge which indicates failure. The final hole diameter is then measured, to calculate the hole expansion ratio (HER).

Based on the ISO 16630 evaluation standard and extensive research, it has been found that multiphase steels, composed of two or more types of phases, such as ferrite, bainite, martensite, et al., evaluate excellent hole expansion performance in advanced high-strength steels (AHSS) [8-10]. Scott et al. [11] and Wu et al. [12] found that optimizing the hole expansion performance of CP steels can be achieved by reducing the strength of

hard phases, such as martensite and MA (martensite-austenite) constituents. Pathak et al. [13] proposed that after punching, voids initiate at the interface between high-hardness phases and the matrix interface, adversely affecting hole expansion performance. Hasegawa et al. [14] observed that cracks propagate along the interface between soft and hard regions during hole expansion, affecting the hole expansion performance. Therefore, weakening the hardness difference between microstructures potentially improves hole expansion performance in multiphase steels. Based on this strategy, some researchers suggest that improving microstructural homogeneity in multiphase steel, and minimizing the interfaces between the soft matrix and hard constituents, are critical to enhancing hole expansion performance [15, 16]. Additionally, the distribution of microstructures influences local mechanical properties, affecting the deformation behavior and the microscopic mechanisms of overall structural fracture [17]. Therefore, this aspect is worthy of further investigation. There are few reports that discuss how microstructure distribution influences hole expansion performance. Nanda et al. [18] suggested that the dispersed distribution of high-hardness MA constituents results in a more uniform local strain distribution within the microstructure, which can delay void nucleation in the steel. The previous research [16] also confirmed that avoiding a chain-like distribution in the matrix can hinder void coalescence into cracks which stabilizes hole expansion performance. However, there are some arguments [19] that introducing banded

* Corresponding author: zhenli_mi@163.com

structures induces altering the crack propagation path and limiting crack expansion in the thickness direction of the sheet, which is beneficial for improving the HER. Our previous work also found that the hole expansion performance could be improved by constructing the continuously distributed MA constituents along the rolling direction at the thickness center in both milling and punching hole conditions. Therefore, it is necessary to study the mechanisms by how the banded structures affect hole expansion behavior.

In this present work, we prepared the banded structures using a hot rolling process and obtained two phases with subtle hardness differences for comparative analysis by controlling the coiling holding temperature. The reason for selecting the hot rolling process is that a better rolling orientation of the banded structures can be obtained by the two-phase rolling, it is also relatively more environmentally friendly and has the prospect of grafting with the thin slab continuous casting and rolling and other short processes if it works satisfying. Hole expansion experiments were conducted to directly observe the hole edge at the thickness position, allowing for an analysis of the microstructural evolution at the hole edge after the expansion. Moreover, an analysis of the fracture morphology from the hole expansion tests was performed to evaluate the influence of microstructure on the hole expansion performance and fracture behavior of experimental steels without and with pre-damage.

2 Methods and procedures

2.1 Materials

The experimental steel was cast into a 50 kg ingot and forged as a 10 cm thickness bulk with the chemical composition (wt.%) of 0.15C-1.5Si-2Mn-0.4Cr-0.18Mo-Fe. The steel was held at 1250 °C for 1.5 h before hot rolling to ensure chemical homogeneity. Then the steel was reduced to around 2 mm by hot-rolling in five passes. In order to obtain the banded structures, the finish temperature of the hot rolling was set to 880 °C since the A_3 temperature of the experimental steel is around 920 °C according to the dilatometer test. The isothermal holding was performed in two temperature variants for 2 h at 650 and 450 °C, respectively, which is aimed at maintaining different phases in banded structures.

2.2 Mechanical property analysis

The tensile specimens were manufactured to a standard dog-bone shape with a gauge length of 25 mm and a width of 6 mm. The longitudinal axes of the samples are parallel to the rolling direction. The uniaxial tensile tests were carried out on the universal tensile testing machine (CMT5605) with a tensile rate of 1 mm/min at ambient temperature.

The hole expansion tests were conducted on a sheet metal forming testing machine (BUP60) in accordance with the ISO 16630 standard. The specimens were 90 mm × 90 mm square sheets with a 10 mm diameter hole

(D_0) punched in the center. Since the sheet thickness was less than 2 mm after surface polishing, the punching clearance was set to $12 \pm 2\%$. A 60° conical tip punch expands the hole in the specimen with the burr side of the hole facing upwards at a punch speed of 0.2 mm/s. A clamping force of 50 kN was applied to the specimen to prevent slipping. The test was terminated when the entire crack had fully propagated through the thickness of the sheet. More than 5 parallel samples were used for each test to control the dispersion of HER. HER is calculated as:

$$HER = (D - D_0) / D_0 \times 100\% \quad (1)$$

where D is the diameter of the hole after failure; and D_0 is the initial diameter; HER represents the hole expansion ratio, with the calculated result taken as an average. Additionally, to investigate the relationship between the microstructure and hole expansion performance while excluding severe shear deformation from punching that could plastically damage the microstructure [16], a batch of holes of specimens was machined by milling. The hole expansion tests were conducted under conditions identical to those for the punched specimens.

2.3 Microstructural characterization

Steel samples were sectioned and cut into small pieces with the dimensions of 6 mm × 8 mm × thickness. Then, the samples were ground with silicon carbide abrasive papers, ranging from 400 to 2000 grit. Next, the specimens were mechanically polished with 1.0 μm diamond polishing paste to remove the scratches caused by grinding. Finally, the surface of each sample was etched with 4 vol.% Nital reagents for 10 seconds to reveal the metallographic features of different phases. The macroscopic fracture morphology and optical microstructure were characterized by a laser confocal microscope (OLS4100). A FEI thermal field emission scanning electron microscope (Quanta FEG 450) equipped with an electron backscatter diffraction (EBSD) detector was applied to observe the SEM specimens in secondary electron (SE-SEM) imaging mode, conducted at the working distance of 10 mm, the accelerating voltage of 15 KeV, and the current of 15 μA. EBSD samples were electrochemically polished at ambient temperature to remove the surface stress layer. The electrolytic polishing solution consists of 10% perchloric acid, 85% ethanol, and 5% propanetriol. EBSD characterization was performed at 20 kV with a step size of 0.06 μm, and AZtecCrystal software was used for data processing.

3 Results and discussion

3.1 Microstructures

Fig. 1 displays the OM and SE-SEM photos of steels which are isothermal holding at 650 °C (IH650) and in 450 °C (IH450). Fig. 1(a, b) confirmed that the banded structures were successfully constructed by the hot rolling process. From the SE-SEM photos, we can see that the IH650 steel mainly contains pearlite and ferrite,

and fewer MA constituents were also characterized. IH450 steel presents lath bainite and martensite. From the continuous cooling phase transformation, since the phase regions of ferrite and pearlite are close to each other, and lath bainite and martensite are equally close either, it seems that the mechanical response among phases in each steel is less different. It has the potential to achieve a higher hole expansion ratio based on former studies where the subtle hardness difference between various microstructures.

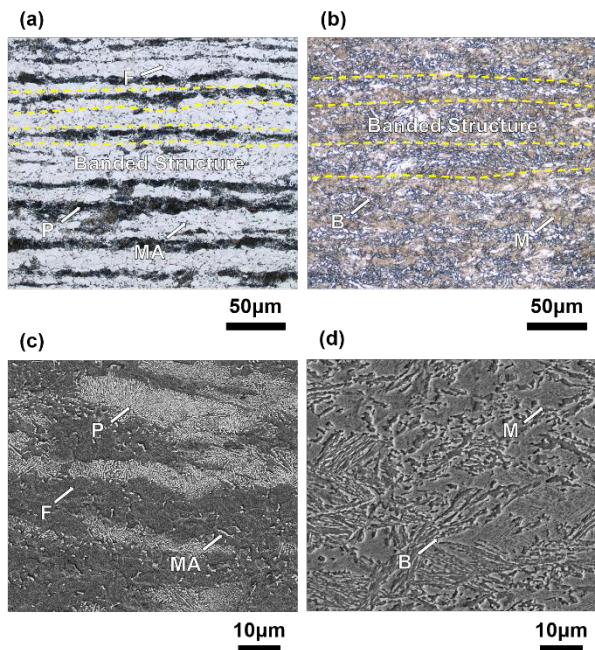


Fig. 1. (a, b) OM and (c, d) SE-SEM photos of (a, c) IH650 steel and (b, d) IH450 steel. P: pearlite, F: ferrite, B: bainite, M: martensite, MA: martensite-austenite constituents.

3.2 Mechanical properties

Fig. 2 shows the tensile stress-strain curves of the 650 °C(IH650) and 450 °C (IH450) isothermal holding steel. The yield strength (YS), ultimate tensile strength (UTS), total elongation (TE), and HER in milling and punching hole conditions are listed in Table 1.

IH650 steel balances well in strength and ductility which obtain a product of strength and elongation around 20 GPa%. The combination of pearlite and ferrite should take responsibility for this high performance. IH650 steel also exhibits an excellent HER in milling and punching conditions in terms of strength level compared to previous studies [16, 20]. IH450 steel performs well in strength while short in both elongation and HER. Although the dual phases are close to each other and the distribution of structures is prone to resist the crack propagation in hole expansion deformation theoretically, it is still unsatisfied in hole expansion property. It is reasonable to say that the applicability of the microstructures homogeneity strategy in improving hole expansion performance is limited by the hard and low-temperature transformation phases such as lath bainite and martensite no matter what sophisticated structural design has been made. The framework composition of phases is crucial in hole expansion behavior.

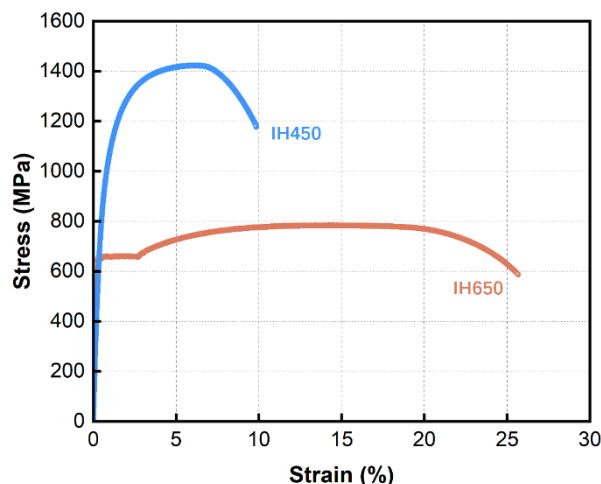


Fig. 2. The tensile stress-strain curves of the IH650 and IH450 steel.

Table 1. Mechanical properties of experimental steels.

	YS (MPa)	UTS (MPa)	TE (%)	HER (%)	
				punch	milling
IH650	651 ± 2	788 ± 3	26 ± 2	34 ± 2	135 ± 2
IH450	943 ± 12	1419 ± 5	12 ± 2	9 ± 2	33 ± 2

3.3 The microstructures in hole expansion behavior without pre-damage

In order to figure out the effect of microstructures on hole expansion deformation, further investigations were applied on both steels in milling conditions, which could eliminate the interference of process factors (pre-damage). Fig. 3 shows EBSD maps of both steels along the cross-section from the hole edge to the undeformed matrix (Fig. 3(a)). We could directly see the damaged condition of microstructures from the edge of the hole to the deformed matrix by the occupancy and location of the unidentified black dots. Overall, the damage is most drastic near the edge of the hole as Fig. 3(b1, c1).

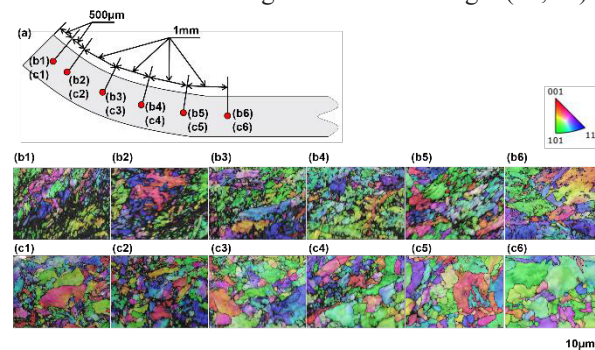


Fig. 3. EBSD maps of (b1~b6) IH650 and (c1~c6) IH 450 steel along (a) the cross-section from hole edge to undeformed matrix, scan positions are shown as red regions.

For the IH650 steel, the black area of damage divides the matrix into many small 1~2 µm grains, while bypassing the interior large pearlite grains containing low misorientation boundaries, as is evident in Fig. 3(b1, b2). In Fig. 3 (b4, b5), against the microstructural morphology shown in Fig. 1 (c), the damaged areas are

prone to locate at the grain boundaries of the ferrite, and the grains are deformed and elongated along the deformation direction. There's hardly to see damage or deformed grains 5 mm away from the hole edge as shown in Fig. 3(b6). In IH450 steel, damage areas are distributed along the small size of grains which could be identified as the interface of bainite and martensite according to Fig.1 (d). It can be seen from Fig. 3 (c5, c6) that the damage is almost invisible at 3 mm away from the edge of the hole, which is related to the smaller deformation area with the small punch displacement of the IH650 steel. Compared to IH450 steel, the damage in IH650 steel appears to be more severe, but it has a higher HER, which means that the microstructure of IH650 has a better ability to take on the deformation even after the damage (necking) has occurred.

Fig. 4 could help to explain why the microstructures in IH650 steel have the ability to endure deformation after damage. A crack that did not penetrate the thickness was captured on the hole edge shown in Fig. 4(a). In a lower magnification (Fig. 4(b)), it can be clearly seen that the crack instead of having the shortest path to expand perpendicular to the thickness or at a 45-degree angle to the thickness direction, the cracks acted along the circumferential direction for about 50 μm during expansion, enlarged as shown in Fig. 4(c). Figure 4(d) shows the damage adjacent to the crack tip, where a number of deformed elongated voids can be seen ahead of the main crack propagation direction, which have a tendency to coalesce into microcracks. These voids are usually located at the interface of pearlite and ferrite, or next to MA islands. Due to the banded microstructure, these void-prone interfaces are also distributed along the rolling direction (described as circumferential in this case at the hole edge). These pre-formed damages next to the crack tip induce the direction of crack propagation, which is in the circumferential direction. This phenomenon is also confirmed in Fig. 3(b1~b6). Besides, from the strain stress curves (Fig. 2), the post elongation and toughness of IH650 steel is higher than IH450 steel, which could explain its high deformation capacity after necking.

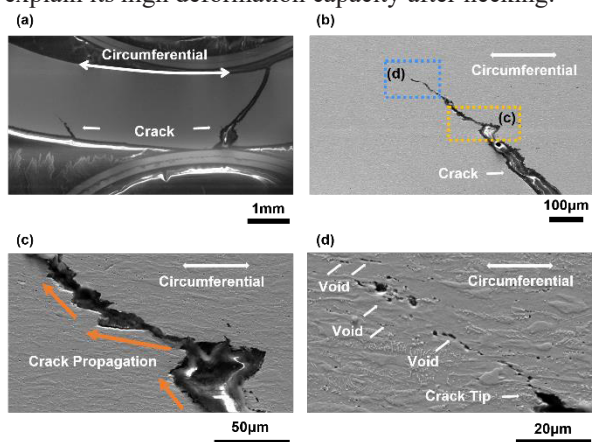


Fig. 4. The SEM-SE microstructures on the hole edge surface of the IH650 steel after hole expansion.

3.4 The evaluation of microstructures in hole expansion behavior with pre-damage

From the above investigation, we understand that the IH650 steel performs well in hole expansion without pre-damage hole since the pearlitic and ferrite with MA constituents banded structure facilitates crack circumferential propagation, while the soft ferrite and pearlite also have a better deformation capacity compared to the lath bainite and martensite in IH450 steels. However, we know that the processing of the hole affects the surface quality, which will largely affect the hole expansion performance [21, 22]. For the IH650 and IH450 steel studied in this paper, the authors in the processing of milling hole specimens found that if the direction of the surface abrasion is perpendicular to the rolling direction, relative to parallel to the rolling direction of the abrasion specimen HER of an average of 15% higher, even if there is no hardness gradient or damage on the edge of the hole in both cases. The reason is that the abrasion marks are equivalent to pre-constructed surface damage so the banded structures in the rolling direction of the hole edge are weak and prone to crack. It is necessary to examine the microstructure damage at the edge of the hole after punching is necessary.

Fig. 5 shows the SEM-SE photos of the initial hole internal surface of steels. After hole punching, the initial hole surface was characterized by the rollover zone, burnished zone, fracture zone, and burr, as shown in Fig. 5(a, b). In the burnished zone, many 1~3 μm microvoids were observed in IH650 steel (Fig. 5c), while streamlined microstructures were mainly occupied in IH450 steel (Fig. 5d). The authors' previous study observed that the appearance of streamlined microstructure along the thickness direction at the hole surface is the first step in the evolution of microstructures deformation during hole expansion, after which the streamlined structures will twist due to the pinning of hard phases (i.e., MA constituents), forming many microcracks that ultimately induce fracture. In IH450 steel, the damage caused by punching makes the initial hole expansion deformation skip the streamlined structures formation process in the deformation stage, hence, the deformation process is accelerated, which makes the HER of the pre-damaged steel always lower than that without the pre-damaged steel. Some studies [13, 23] considered that the void defects may be expected to act as crack initiation sites, and will severely affect the subsequent hole expansion results. However, in the present work, the hole expansion performance of IH650 steel was better than IH450 steel, and the authors suggest that possibly the loss of HER by the voids is not more serious than the loss of HER by the appearance of streamlined structures, which may be related to the fact that streamlined structures eventually evolves into microcracks. This part of the inference needs further experimental confirmation.

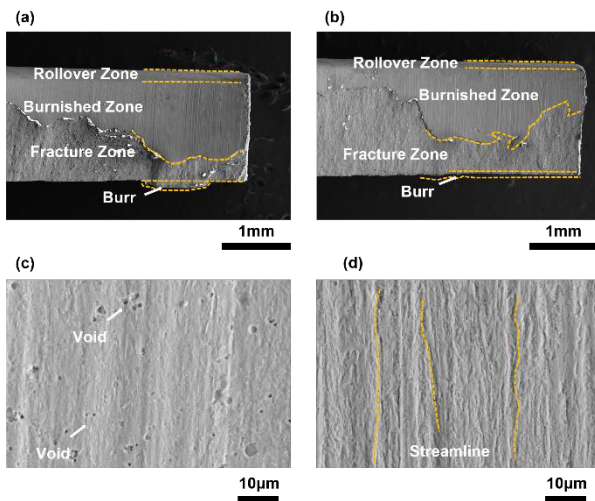


Fig. 5. SEM micrographs of the initial hole surface. Overview of through-thickness initial hole surface of (a) IH650 steel, (b) IH450 steel, and closer observation of burnished zone (c) IH650 steel, and (d) IH450 steel.

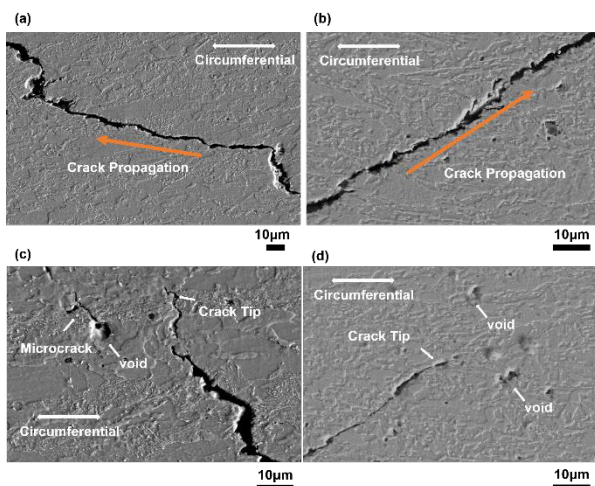


Fig. 6. The SEM-SE microstructures on the hole edge surface of the (a, c) IH650 steel, and (b, d) IH450 steel after hole expansion.

The crack on the hole edge surface of the IH650 and IH450 steel is displayed in Fig. 6. As shown in Fig. 6(a), the crack propagates along the circumferential direction during expansion just similar to the observation in Fig. 4(c), here the cracks extend through the interior of the pearlite in addition to along the interface, while in IH450 steel the crack propagates at around 45° along the circumference (Fig. 6(b)). As present in Fig. 6(c), there are microcracks near the crack tip that pass through the interior of the pearlite in I650 steel, and the microcracks are connected to the void. This void is different from the void formed by deformation (Fig. 4(d)), and its morphology is consistent with the size and morphology of the voids produced by punching (Fig. 5(c)). Moreover, this microcrack is not observed in the steel without pre-damage (Fig. 4), and it is assumed that the formation of microcracks passing through the pearlitic is related to these punching voids. Further, the circumferential crack propagation is related to the formation of cracks within the banded pearlitic, which may have further lengthened the depth of circumferential propagation of the cracks. There are no obvious instructions for crack propagation

in IH450 steel (Fig. 6(d)) since it seems the main crack is made up of many deformed voids and microcracks connected and is related to the strength and toughness of the matrix.

4 Conclusions

In this work, two types of banded structures steels were constructed and their hole expansion behavior with and without pre-damage was investigated. Among them, the steels with banded ferrite and pearlite have excellent hole expansion performance because they still possess strong deformation capacity after necking. The cracks extending circumferentially along the direction of the banded structures and the higher toughness of the matrix are responsible for the higher hole expansion performance. Besides, the constituent of structures is crucial since the hard phases such as lath bainite and martensite dominate the hole expansion performance no matter what sophisticated structural design has been made. The combination of ferrite and pearlite banded structures is an outstanding microstructure that has the potential to inspire the development of advanced high-strength and hole expansion requirement multiphase steels. It should be noted that the sensitivity of demand applications to anisotropy should be considered and evaluated before presenting the band structure in steel.

References

1. A. W. Hudgins, D. K. Matlock, *Mater. Sci. Eng., A* **654**,169 (2016).
2. C. Lesch, N. Kwiaton, F. B. Klose, *Steel Res. Int.* **88**,1700210 (2017).
3. S. K. Paul, *Materialia* **9**,100566 (2020).
4. M. Feistle, R. Golle, W. Volk, *J. Mater. Process. Technol.* **302**,117488 (2022).
5. N. Pathak, C. Butcher, M. Worswick, *J. Mater. Eng. Perform.* **25**,4919 (2016).
6. R. S. Bharathy, T. Venugopalan, M. Ghosh, *Metallogr., Microstruct., Anal.* **12**,74 (2023).
7. A. C. S. Reddy, S. Rajesham, P. R. Reddy, A. C. Umamaheswar, *AIP Conf. Proc.* **2269**,030026 (2020).
8. E. Song, G. H. Lee, H. Jeon, B. J. Park, J. G. Lee, J. Y. Kim, *Mater. Sci. Eng., A* **817**,(2021).
9. P. Efthymiadis, S. Hazra, A. Clough, R. Lakshmi, A. Alamoudi, R. Dashwood, B. Shollock, *Mater. Sci. Eng., A* **701**,174 (2017).
10. J. Hu, L.-X. Du, J.-J. Wang, *Mater. Sci. Eng., A* **554**,79 (2012).
11. C. P. Scott, B. Shalchi Amirkhiz, I. Pushkareva, F. Fazeli, S. Y. P. Allain, H. Azizi, *Acta Mater.* **159**,112 (2018).
12. Y. Wu, J. Uusitalo, A. J. Deardo, *Mater. Sci. Eng., A* **828**,(2021).
13. N. Pathak, C. Butcher, M. J. Worswick, E. Bellhouse, J. Gao, *Materials* **10**,(2017).

14. K. Hasegawa, K. Kawamura, T. Urabe, Y. Hosoya, *ISIJ Int.* **44**,603 (2004).
15. D. Frómeta, N. Cuadrado, J. Rehr, C. Suppan, T. Dieudonné, P. Dietsch, J. Calvo, D. Casellas, *Mater. Sci. Eng., A* **802**,140631 (2021).
16. X.-Y. Yang, Y.-G. Yang, X. Fang, H.-L. Zhang, Z.-L. Mi, *J. Iron Steel Res. Int.* (2023).
17. L. Lan, M. Yu, C. Qiu, *Mater. Sci. Eng., A* **742**,442 (2019).
18. T. Nanda, V. Singh, G. Singh, M. Singh, B. R. Kumar, *Arch. Civ. Mech. Eng.* **21**,1 (2021).
19. Y. Wang, Y. Xu, X. Wang, J. Zhang, F. Peng, X. Gu, Y. Wang, W. Zhao, *Mater. Sci. Eng., A* **852**,143722 (2022).
20. X. Chen, H. Jiang, Z. Cui, C. Lian, C. Lu, *Procedia Eng.* **81**,718 (2014).
21. A. Karellova, C. Kremaszky, E. Werner, T. Hebesberger, A. Pichler, **1**,156 (2007).
22. K. Jeong, Y. Jeong, J. Lee, C. Won, J. Yoon, *Materials* **16**,(2023).
23. Y. Wu, J. Uusitalo, A. J. Deardo, *Mater. Sci. Eng., A* **828**,142070 (2021).